Supplement of Solid Earth, 16, 1181–1204, 2025 https://doi.org/10.5194/se-16-1181-2025-supplement © Author(s) 2025. CC BY 4.0 License.





Supplement of

Dissolution-precipitation creep in polymineralic granitoid shear zones in experiments – Part 1: Strain localization mechanisms

Natalia Nevskaya et al.

Correspondence to: Natalia Nevskaya (natalia.nevskaya@yale.edu)

The copyright of individual parts of the supplement might differ from the article licence.

S 1: TEM XRD maps and SEM images used for interpretations

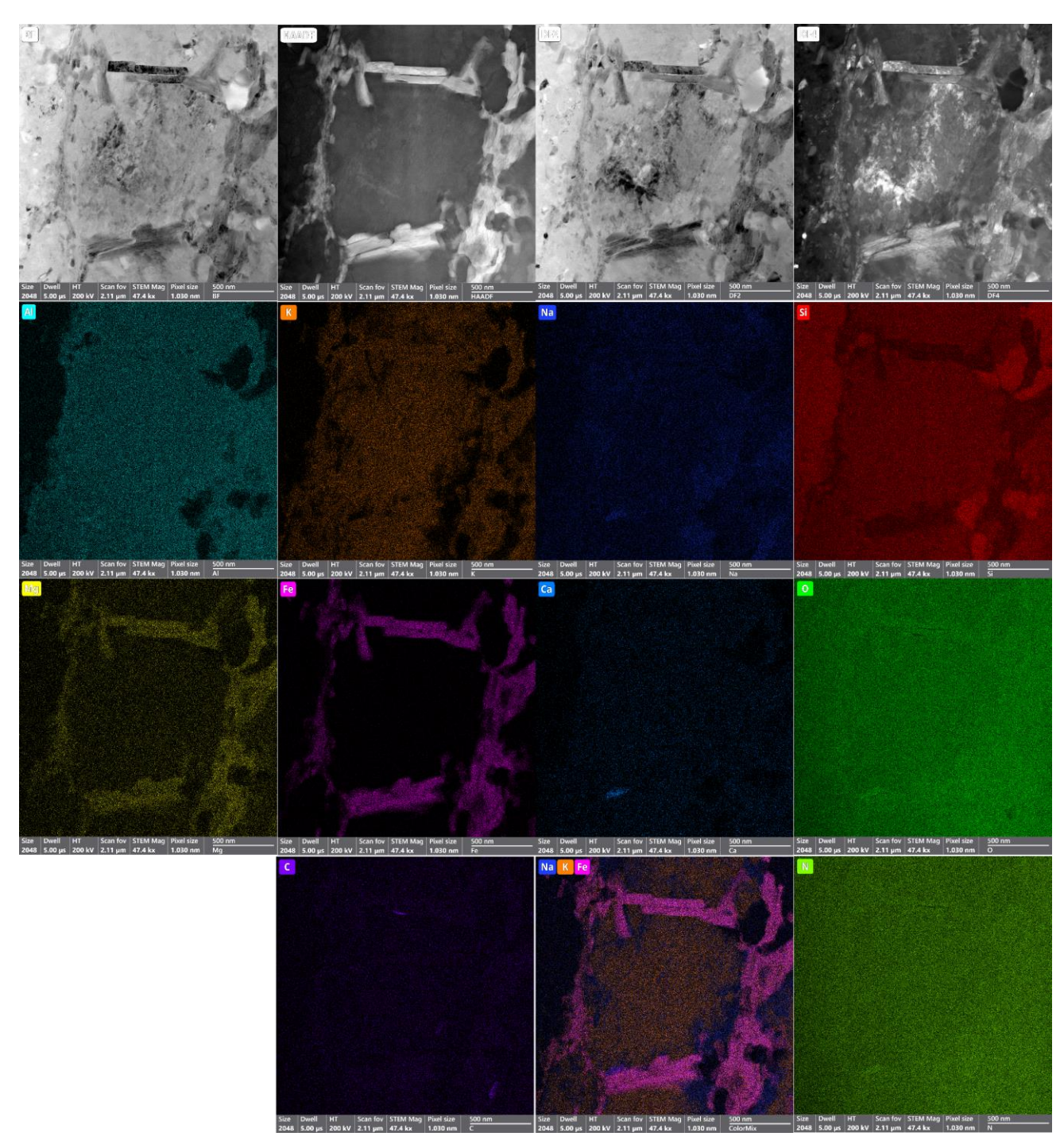


Fig. S1: STEM Map in foil 1 used for Fig. 6. Experiment No. 618NW, Type I with pre-fracture. Key observation is the chemical changes occurring to the K-fsp grain overgrown by biotite. Note that the K-fsp most likely is a primary grain, as it displays a very high dislocation density.

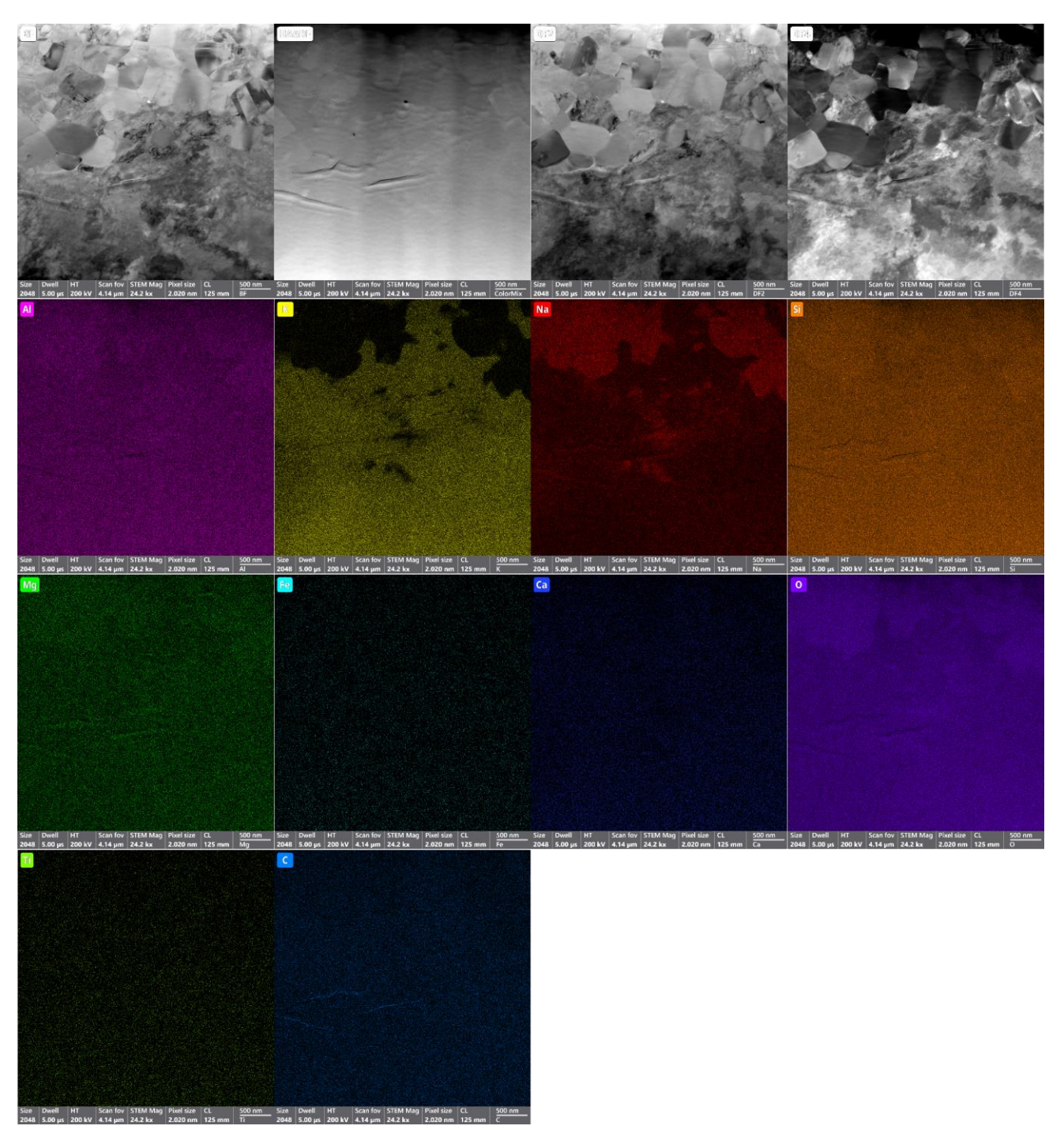


Fig.S2: STEM Map used for Fig. 8. Experiment No. 670NW, Type II without pre-fracture. The chemical maps show that at the boundary of albite and K-feldspar, new equigranular grains with low dislocation density have formed. Furthermore, chemical changes of K-depletion and Na-enrichment occur in the primary K-feldspar grain.

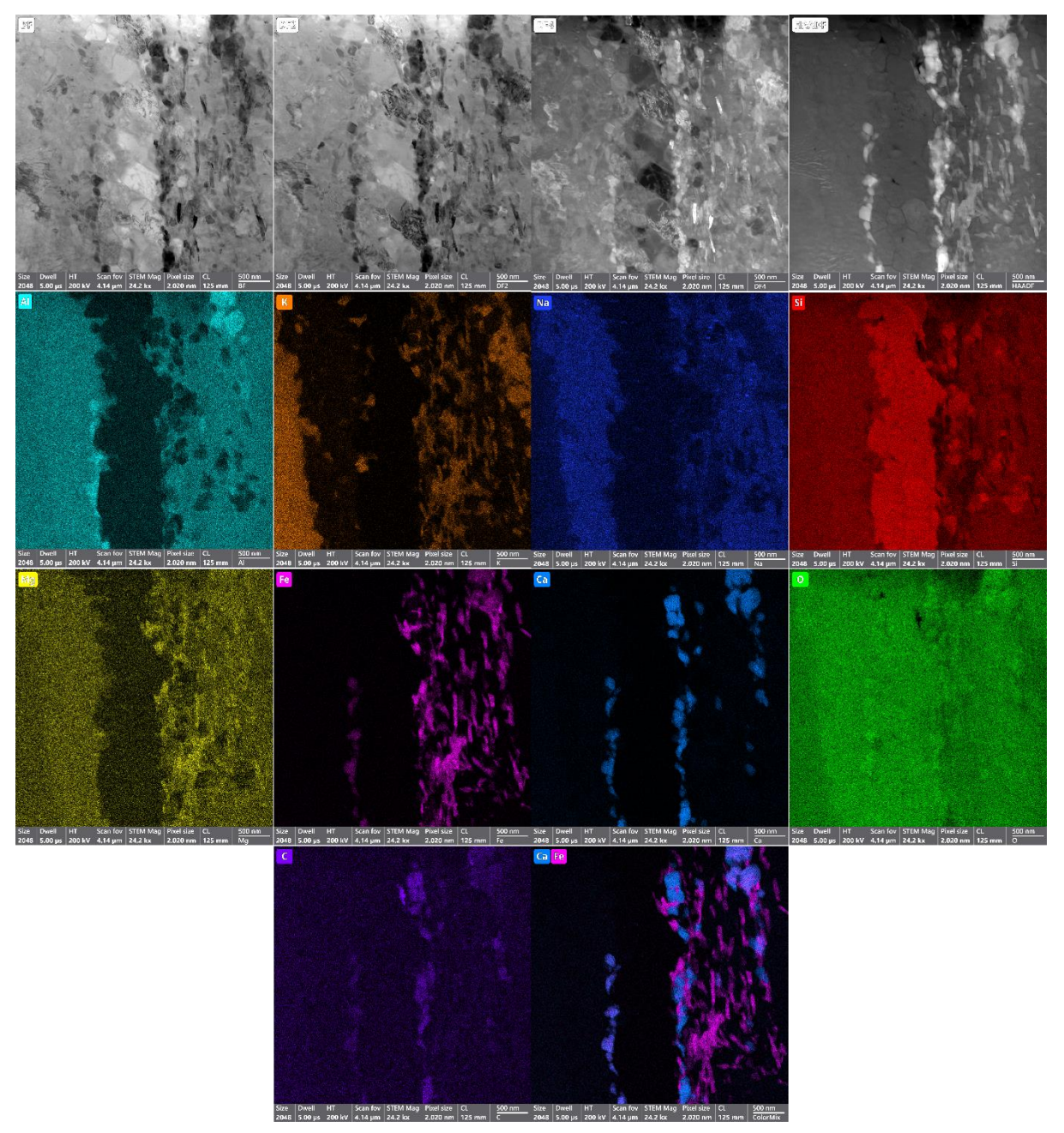
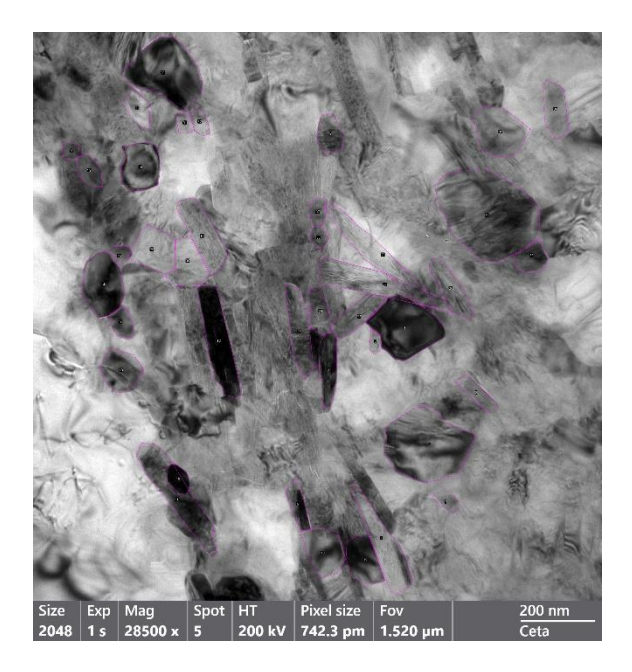
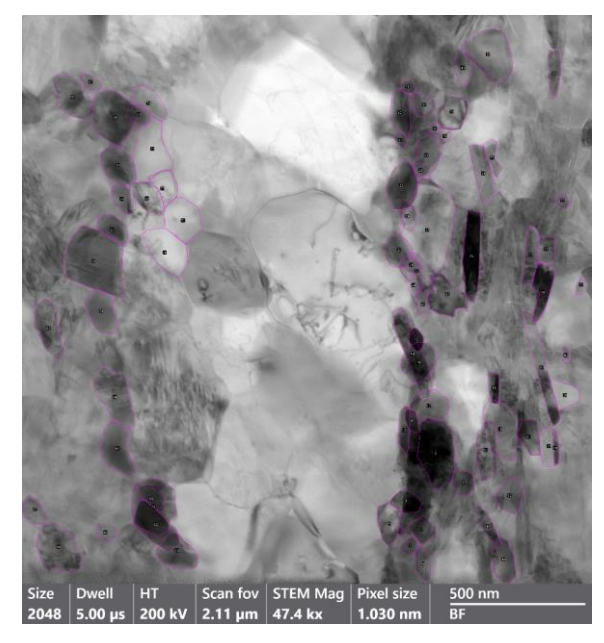


Fig. S3: Additional chemical maps from STEM in sample 618NW (TEM foil location 1, as indicated in Fig. 6). This is an example, where a lens of coarser quartz is surrounded by very fine-grained Mg-, K- and Fe-rich mineral grains (biotite) and Ca- and C- rich grains (calcite) that have nucleated during the experiment (the upper right hand grains are clinozoisites). Note also the alignment of elongated grains parallel to the shear zone orientation.





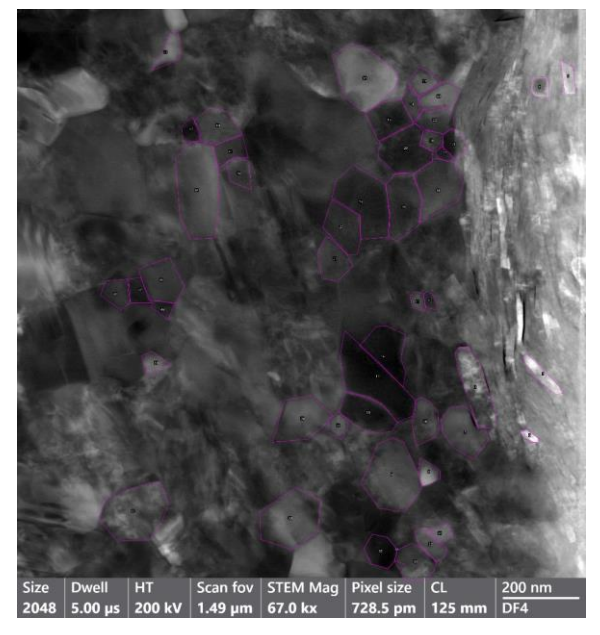


Fig. S4: Example STEM images for grain size analysis of medium to high strain samples, in experimental sample 618NW (TEM foil location 1, as indicated in Fig. 6).

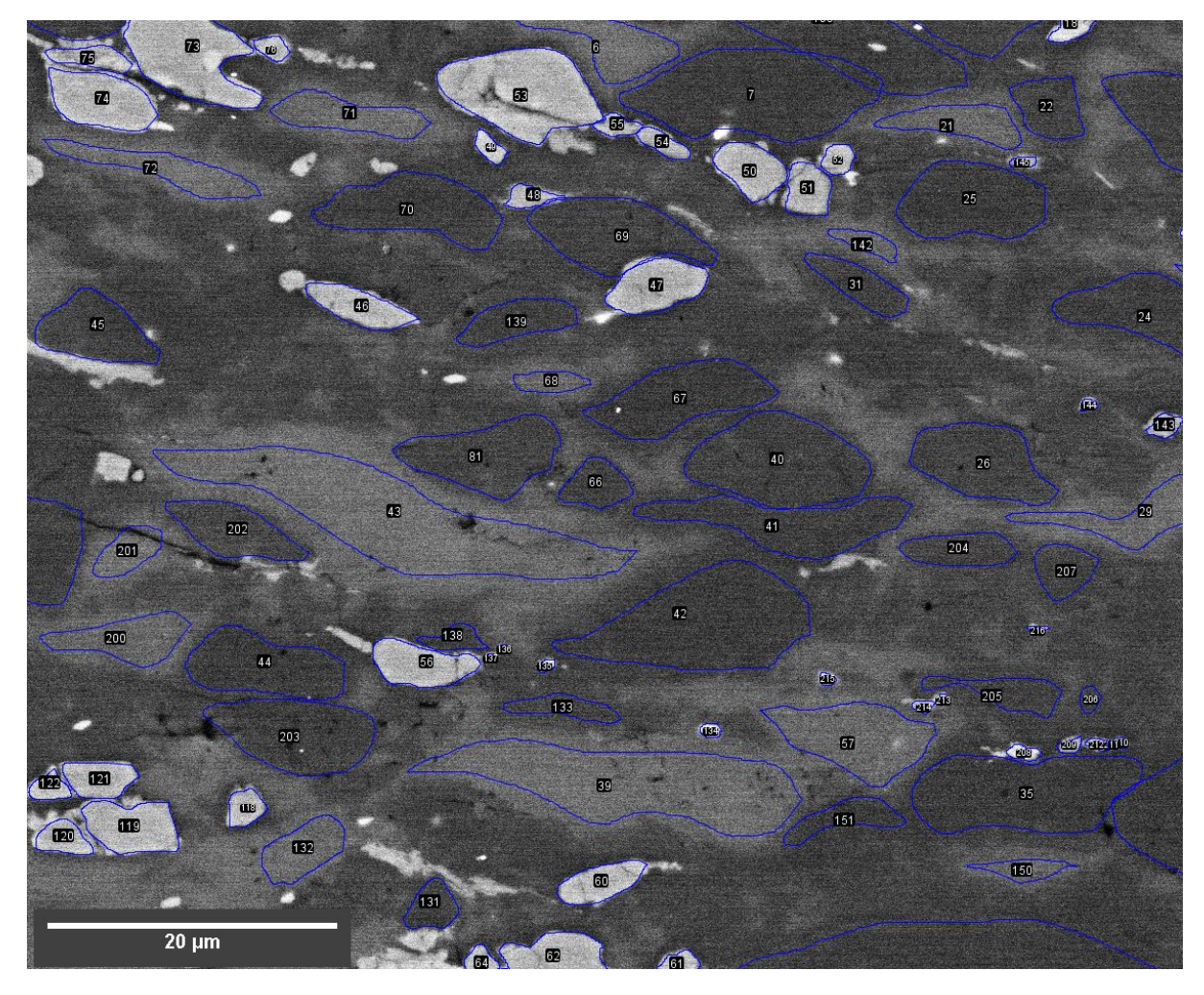


Fig. S5: Example SEM image for grain size analysis and grain elongation at high strain of Type II experiment 670NN. The grey shade and fading phase boundaries are locations where TEM has shown DPC occurs at phase boundaries and there are very fine grains not to be resolved with SEM.

S2: Melt or no melt

Petrological (melting) experiments predict that granitic rocks may melt at 1.2 GPa and 650°C with the presence of water (Holtz, 2001). For melting to occur, a eutectic composition is necessary: quartz, albite, K-feldspar, and water in contact. In our experiments, it is rarely the case that all these components are in contact at a grain triple junction. No melt-pockets at such locations have been observed. Mostly, albite and K-feldspar are in contact, and the melting temperature of these pure feldspar systems is higher (>700°C). Therefore, eutectic melting of the ultramylonite is excluded as it is not observed on the nanometer scale.

Several granitic studies reported melt or partially amorphous material in granitic systems, but mostly at higher P,T-conditions (Dell'Angelo et al., 1987; Dell'Angelo and Tullis, 1988; Pec et al., 2016; Pec and Al Nasser, 2021). There are several reasons why in our samples melt was not detected and has no influence on the strength or microstructural evolution. In, e.g., Young et al. (2022), recrystallized pseudotachylites are distinguished from ultramylonites by 12 criteria (Young et al., 2022), none of which are observed in our experiments. On the contrary, all the grains are crystalline and show typical ultramylonitic microstructures down to 10's of nanometers, as has been confirmed through TEM imaging (Figs. 6, 8). Not even partially amorphous material was identified (as in Pec et al., 2016; Pec and Al Nasser, 2021). The only amorphous grain boundaries that were observed in TEM images (in supplementary material) occurred in the sample during imaging by beam amorphization. The main reason why amorphous material is absent in our samples is most likely given by the far lower differential stresses in our experiments compared to those by Pec (2016) and Al Nasser, (2021). The mechanical amorphization is favored by high stresses.

Additionally, one additional experiment was performed with an increased added H_2O amount of 0.5wt% (exp. 654NN, Appendix Table in PhD Thesis Nevskaya, 2024). Theoretically, the increased H_2O amount should have increased the melt content, making it easier to observe. However, no evidence for melt was found in this sample either after thorough SEM-investigations.

The absence of melt is in agreement with other deformation experiments on granitoid rocks at similar P,T-conditions, where no melt has been documented (Tullis, 2002; Tullis et al., 1990). Even if there were melt pockets that were overlooked during high resolution and high magnification imaging, there is no evidence for throughgoing melt films that would affect the rheology significantly. We cannot exclude melt in an initial stage, which could have been produced by local stress concentrations but any potentially present melt has crystallized instantly due to its kinetics, because it would crystallize as soon as there is a slight stress drop. Therefore, we do not consider any influence of melt on our experimental observations.

S3: Energy flux calculations

Table S1: Values for calculating the energy fluxes for the assumed deforming sample volume in Type I and Type II experiments as described in section 4.2.2.

Sample	Strain rate (s ⁻¹)	Differential/ shear stress (Pa)	Deformation volume (m³)	Energy flux (J/s)
Localized strain (618NW)	1.23E-03	≈260000	6.23E-10	2.0E-07
Pure shear (bottom 2/3) (670NW)	2.01E-06	≈200000	2.50E-07	1.0E-07